

Optical bistability and cutoff solitons in photonic bandgap fibers

Marin Soljačić, Eleftherios Lidorikis, Mihai Ibanescu, Steven G. Johnson, and
J.D. Joannopoulos

Department of Physics, MIT, Cambridge 02139, USA
marin@alum.mit.edu

Yoel Fink

Department of Material Science and Engineering, MIT, Cambridge 02139, USA

Abstract: We present detailed theoretical and numerical analysis of certain novel non-linear optical phenomena enabled by photonic bandgap fibers. In particular, we demonstrate the feasibility of optical bistability in an axially modulated nonlinear photonic bandgap fiber through analytical theory and detailed numerical experiments. At 1.55 μm carrier wavelength, the in-fiber devices we propose can operate with only a few tens of mW of power, have a nearly instantaneous response and recovery time, and be shorter than 100 μm . Furthermore, we predict existence of gap-like solitons (which have thus far been described only in axially periodic systems) in axially uniform photonic bandgap fibers.

© 2004 Optical Society of America

OCIS codes: (190.1450) Bistability; (060.5530) Pulse propagation and solitons; (190.4370) Nonlinear optics, fibers; (230.4320) Nonlinear optical devices

References and links

1. P. Russell, "Photonic crystal fibers," *Science* **299**, 358-362 (2003).
2. Y. Fink, D. J. Ripin, S. Fan, C. Chen, J. D. Joannopoulos, and E. L. Thomas, "Guiding optical light in air using an all-dielectric structure," *J. Lightwave Technol.* **17**, 2039-2041, (1999).
3. Steven G. Johnson, Mihai Ibanescu, M. Skorobogatiy, Ori Weisberg, Torkel D. Engeness, Marin Soljačić, Steven A. Jacobs, J. D. Joannopoulos, and Yoel Fink, "Low-loss asymptotically single-mode propagation in large-core OmniGuide fibers," *Opt. Express* **9**, 748-779, (2001).
4. S.D.Hart, G.R.Maskaly, B.Temelkuran, P.H.Prideaux, J.D.Joannopoulos, Y.Fink, "External Reflection from Omnidirectional Dielectric Mirror Fibers," *Science* **296**, 510-513, (2002).
5. B. Temelkuran, S.D. Hart, G. Benoit, J.D. Joannopoulos, and Y. Fink, "Wavelength-scalable hollow optical fibres with large photonic bandgaps for CO₂ laser transmission," *Nature* **420**, 650-653, (2002).
6. B.E.A.Saleh, and M.C.Teich, *Fundamentals Of Photonics* (John Wiley&Sons, 1991).
7. Marin Soljačić, Mihai Ibanescu, Steven G. Johnson, Yoel Fink, and J.D.Joannopoulos, "Optimal Bistable Switching in Non-Linear Photonic Crystals," *Phys. Rev. E* **66**, 055601(R) (2002).
8. J.S.Foresi, P.R.Villeneuve, J.Ferrera, E.R.Thoen, G.Steinmeyer, S.Fan, J.D.Joannopoulos, L.C.Kimerling, H.I.Smith, and E.P.Ippen, "Photonic-bandgap microcavities in optical waveguides," *Nature* **390**, 143-145, (1997).
9. Marin Soljačić, Mihai Ibanescu, Steven G. Johnson, J.D.Joannopoulos, and Yoel Fink: "Optical Bistability in Axially Modulated OmniGuide Fibers," *Opt. Lett.* **28**, 516-518, (2003).
10. Steven G. Johnson and J. D. Joannopoulos, "Block-iterative frequency-domain methods for Maxwell's equations in a planewave basis," *Opt. Express* **8**, 173-190, (2001), <http://www.opticsexpress.org/abstract.cfm?URI=OPEX-8-3-173>.
11. For a review, see A.Taflove, *Computational Electrodynamics: The Finite-Difference Time-Domain Method* (Artech House, Norwood, Mass., 1995).
12. H.A.Haus, *Waves And Fields in Optoelectronics* (Prentice-Hall, Englewood Cliffs, NJ, 1984).

13. S.G.Johnson, S.Fan, A.Mekis, and J.D.Joannopoulos, "Multipole-cancellation mechanism for high-Q cavities in the absence of a complete photonic band gap," *Appl. Phys. Lett.* **78**, 3388-3390, (2001).
14. G. Lenz, J. Zimmerman, T. Katsufuji, M. E. Lines, H. Y. Hwang, S. Spälter, R. E. Slusher, S.-W. Cheong, J. S. Sanghera, and I. D. Aggarwal, "Large Kerr effect in bulk Se-based chalcogenide glasses," *Opt. Lett.* **25**, 254-256, (2000).
15. Jeffrey M. Harbold, F. Ömer Ilday, Frank W. Wise, and Bruce G. Aitken, "Highly Nonlinear Ge-As-Se and Ge-As-S-Se Glasses for All-Optical Switching," *IEEE Photon. Technol. Lett.* **14**, 822-824, (2002).
16. S.Coen and M.Haelterman, "Competition between modulational instability and switching in optical bistability," *Opt. Lett.* **24**, 80-82, (1999).
17. Stojan Radić, Nicholas George, and Govind P. Agrawal, "Theory of low-threshold optical switching in nonlinear phase-shifted periodic structures," *J. Opt. Soc. Am. B* **12**, 671-680, (1995).
18. J.E.Heebner, and R.Boyd, "Enhanced all-optical switching by use of a nonlinear fiber ring resonator," *Opt. Lett.* **24**, 847-849, (1999).
19. A.Yariv, "Critical coupling and its control in optical waveguide-ring resonator systems," *IEEE Photon. Technol. Lett.* **14**, 483-485, (2002).
20. C.Kerbage, and B.J.Eggleton, "Microstructured Optical Fibers," *Optics&Photonics News* 38-42, (September 2002).
21. H.G. Winful, J.H. Marburger, and E. Garmire, "Theory of bistability in nonlinear distributed feedback structures," *Appl. Phys. Lett.* **35**, 379-381, (1979).
22. Wei Chen and D.L. Mills, "Gap solitons and the nonlinear optical response of superlattices," *Phys. Rev. Lett.* **58**, 160-163, (1987).
23. C. Martijn de Sterke and J.E. Sipe, "Envelope-function approach for the electrodynamics of nonlinear periodic structures," *Phys. Rev. A* **38**, 5149-5165, (1988).
24. D.N. Christodoulides and R.I Joseph, "Slow Bragg solitons in nonlinear periodic structures," *Phys. Rev. Lett.* **62**, 1746-1749, (1989).
25. C. Martijn de Sterke and J.E. Sipe, "Switching dynamics of finite periodic nonlinear media: A numerical study," *Phys. Rev. A* **42**, 2858-2869, (1990).
26. B.J. Eggleton, C. Martijn de Sterke, and R.E. Slusher, "Nonlinear pulse propagation in Bragg gratings," *J. Opt. Soc. Am. B* **14**, 2980-2993, (1997).
27. D. Taverner, N.G.R. Broderick, D.J. Richardson, R.I. Laming, and M. Ibsen, "Nonlinear self-switching and multiple gap-soliton formation in a fiber Bragg grating," *Opt. Lett.* **23**, 328-330, (1998).
28. S. Janz, J. He, Z.R. Wasilewski, and M. Cada, "Low threshold optical bistable switching in an asymmetric $\frac{1}{4}$ -shifted distributed-feedback heterostructure," *Appl. Phys. Lett.* **67**, 1051-1053, (1995).
29. Eleferios Lidorikis, Marin Soljacic, Mihai Ibanescu, Yoel Fink, and J.D.Joannopoulos, "Gap solitons and optical switching in axially uniform systems," *Opt. Lett.*, in press.
30. R.F. Gregan, B.J. Mangan, J.C. Knight, T.A. Birks, P.St.J. Russell, P.J. Roberts, and D.C. Allan, "Single-Mode Photonic Band Gap Guidance of Light in Air," *Science* **285**, 1537-1539, (1999).
31. This special kind of modal cutoff is different from the ones found in many simple waveguiding systems which appear very close to the light line ($k \neq 0$) and thus are very lossy (no feedback) and do not have zero group velocity solutions.
32. E. Lidorikis, K. Busch, Qiming Li, C.T. Chan, and C.M. Soukoulis, "Optical nonlinear response of a single nonlinear dielectric layer sandwiched between two linear dielectric structures," *Phys. Rev. B* **56**, 15090-15099, (1997).
33. G. P. Agrawal, *Nonlinear fiber optics* (Academic Press, London, UK, 1995); *Applications of nonlinear fiber optics* (Academic Press, London, UK, 2001).

1. Introduction

Photonic bandgap fibers have already enabled exploring non-linear optical phenomena in many regimes where they were inaccessible before [1]. In this manuscript, we present two designs of devices for ultra-fast all-optical signal processing, based on non-linear photonic bandgap fibers. In Section 2, we present a small (few λ) in-fiber device that can exhibit optical bistability at power levels close to the ones used in telecommunication networks today. In Section 3, we demonstrate existence of gap-like solitons in axially uniform systems. We conclude in Section 4.

2. Optical bistability in axially modulated photonic bandgap fibers

OmniGuide fibers are a new type of cylindrical multi-layer dielectric fibers [2,3] that have only very recently been implemented experimentally [4,5]. Their cladding is an omnidirectional multi-layer mirror that reflects light of any polarization and any direction. These photonic bandgap fibers can have a hollow core and a guiding mechanism that depends only on the cladding. We propose to exploit these facts to obtain much stronger axial optical modulation than is possible in conventional fibers through insertion of material (e.g. spheres) into the core. Moreover, due to strong transverse confinement, much smaller transverse modal areas are possible than in usual low index-contrast fibers. In this way, we show how optimal ultra-fast bistable devices can be achieved with operating powers less than $40mW$, whose highly nonlinear input/output power relation is key to many applications [6] (e.g., all-optical pulse reshaping, optical limiting, logic gates, etc.). Our device retains all the advantages of similar photonic crystal [7] or high index-contrast devices [8] in terms of power, size, and speed. On the other hand, the fact that it is an in-fiber device should make it easier to produce and to couple with another fiber. In this section [9], we solve the full non-linear Maxwell's equations numerically to demonstrate optical bistability in this class of systems. Moreover, we present an analytical model that excellently describes their behavior and is very useful in predicting optimal designs. For concreteness, our analysis focuses on OmniGuide fibers; nevertheless, one should be able to implement all the principles described in this section in any hollow photonic crystal fiber that has a large enough lateral bandgap.

A schematic of a typical design is shown in Fig. 1. It consists of an axially modulated single-mode OmniGuide fiber with a core of diameter $0.41\lambda_0$, where λ_0 is the carrier wavelength in vacuum. The cladding consists of 7 bilayers (periods), each $0.3\lambda_0$ thick, 30% of which thickness is the high index ($n_H=2.8$) material. The inner-most layer, adjacent to the core, is low-index ($n_L=1.5$). The axial modulation consists of 41 ($n_{SPH}=1.5$) spheres tightly filling the core (diameter $0.41\lambda_0$). The periodicity of the axial modulation opens a bandgap for the propagating mode. Our 3D frequency-domain simulations [10] tell us that structures like the one in Fig. 1 easily open axial bandgaps of 6% or larger (vs. $<0.1\%$ in grated silica fibers).

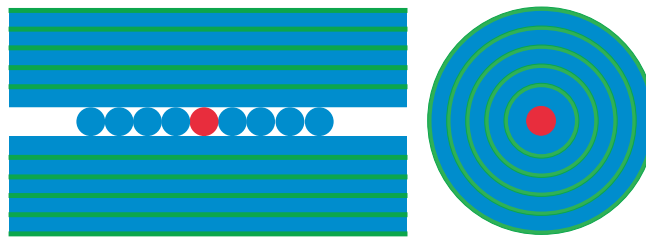


Fig. 1. Schematic of a non-linear OmniGuide device in which we demonstrate optical bistability. The left panel presents a longitudinal cross-section; the panel on the right presents a transverse cross-section.

A defect in the axial periodicity creates a resonant cavity supporting a tightly confined, high-Q resonant mode. In the implementation of Fig. 1, the defect is introduced by changing the index of refraction of the central sphere to $n_{DEF}=1.9$. Tight confinement in the transverse direction is provided by the large band-gap of the OmniGuide cladding, while strong confinement in the axial direction is provided by the large axial bandgap. The cavity couples to the waveguide (axially uniform fiber) through tunneling processes. We model the low-index material to have an instantaneous Kerr non-linearity (the index change is $\delta n(\mathbf{r},t)=cn_L\epsilon_0 n_2 |\mathbf{E}(\mathbf{r},t)|^2$, where n_2 is the Kerr coefficient.)

We perform nonlinear finite-difference time-domain (FDTD) simulations [11], with perfectly matched layers (PML) boundary condition, of this system. These simulations propagate Maxwell's equations exactly, with no approximations apart for the discretization,

and are therefore capable of predicting true experimental results fairly exactly. Due to the cylindrical symmetry of the system in Fig. 1, our system is effectively two-dimensional. Consequently, we can obtain excellent physical understanding of the system by performing 2D FDTD simulations. The numerical values obtained with 2D calculations will differ from the true 3D values only by a geometrical factor of order unity.

The cavity supports a strongly localized resonant mode (transverse modal area $\approx \lambda_0^2/3$ and axial length of the mode $\approx 6\lambda_0$). Note that the transverse modal area is 2 orders of magnitude smaller than in typical low index contrast fibers; one could couple such fibers with tapering. The system has a nearly Lorentzian transmission spectrum: $T(\omega) \equiv P_{OUT}(\omega)/P_{IN}(\omega) \approx \gamma_w^2 / [(\gamma_r + \gamma_w)^2 + (\omega - \omega_{RES})^2]$, where P_{OUT} and P_{IN} are the outgoing and incoming powers respectively, ω_{RES} is the resonant frequency, γ_w is the decay width due to the coupling of the cavity mode to the waveguides, while γ_r is the decay width due to the coupling to the cladding modes [12]. We measure a quality factor $Q = \omega_{RES}/[2(\gamma_r + \gamma_w)] = 540$, and a peak transmission $T_p = 0.88$; from this we obtain that the radiation quality factor $Q_R = \omega_{RES}/2\gamma_r = 8700$. Q_R is finite due to the coupling of energy to the radiating cladding modes; this coupling is the primary cause of losses in our system, but can be controlled [13].

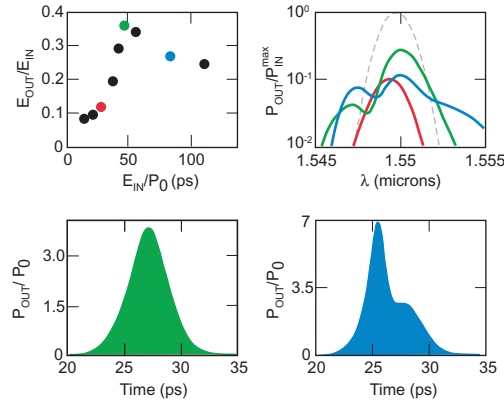


Fig. 2. Numerical experiments with launching temporal-gaussian pulses into the non-linear system of Fig. 1. The upper-left panel shows the transmission as a function of the incoming pulse energy. The colored lines in the upper-right panel display the output spectra for a few pulses, corresponding to the colored dots in the upper-left panel; the spectrum of each pulse is normalized to its peak incoming power; i.e. the input pulse, normalized in the same manner is displayed with the gray dashed line. The lower panels show the output shapes for the incoming pulses denoted with the green, and blue dots in the upper-left panel respectively.

First, we perform numerical experiments in which we launch a series of Gaussian pulses into the system. We choose a carrier frequency $\omega_0 = \omega_{RES} - 3.2(\gamma_w + \gamma_r)$, and the full-width half-maximum (FWHM) bandwidth of our pulses is $\omega_0/FWHM = 796$. The ratio of the transmitted (E_{OUT}) vs. incoming (E_{IN}) pulse energy increases sharply as we approach the bistability threshold, and decreases after the threshold is passed, as shown in the upper-left panel of Fig. 2. Transmitted pulse spectra are also shown for a few pulses in upper-right panel of Fig. 2; the non-linear cavity redistributes the energy in the frequency spectrum; if these changes to the spectrum are undesirable, they can be removed by: optimizing the device, using time-integrating non-linearity, or by adding a frequency-dependent filter to the output of the device. Typical output-pulse shapes are shown in the lower panels of Fig. 2. As one can see in the lower-left panel, even without optimizing our system, we still obtain well-behaved shapes of output pulses in the regime where E_{OUT}/E_{IN} is maximal. Interestingly enough, the output shape is typically less well behaved as the bandwidth of the pulse becomes narrower with respect to the line-width of the cavity. The reason for this is that during the passage through the system,

the pulse observes (self-induced) time-dependent shifts in the resonance position of the cavity, which leave a signature on the pulse itself. It turns out that for shorter-lasting pulses, these signatures get smoothed out. Of course, when the pulse bandwidth becomes larger than the line-width of the cavity, one starts observing distortions for a different reason: in that case, even the linear transmission becomes distorted.

For the case of CW signals we can achieve a precise analytical understanding of bistability in this system, making use of a new fundamental dimensionless characteristic of the cavity, the non-linear feedback parameter κ (derived in detail elsewhere [7]):

$$\kappa \equiv \left(\frac{c}{\omega_{RES}} \right)^d \frac{\int_{VOL} d^d \mathbf{r} \left[|\mathbf{E}(\mathbf{r}) \cdot \mathbf{E}(\mathbf{r})|^2 + 2 |\mathbf{E}(\mathbf{r}) \cdot \mathbf{E}^*(\mathbf{r})|^2 \right] n^2(\mathbf{r}) n_2(\mathbf{r})}{\left[\int_{VOL} d^d \mathbf{r} |\mathbf{E}(\mathbf{r})|^2 n^2(\mathbf{r}) \right]^2 n_2(\mathbf{r})_{MAX}} \quad (1)$$

where $n(\mathbf{r})$ is the unperturbed index of refraction, $\mathbf{E}(\mathbf{r}, t) = [\mathbf{E}(\mathbf{r}) \exp(i\omega t) + \mathbf{E}^*(\mathbf{r}) \exp(-i\omega t)]/2$ is the electric field, $n_2(\mathbf{r})$ is the local Kerr coefficient, VOL of integration is over the extent of the mode, and d is the dimensionality of the system in question. As can be seen from Eq.(1), κ is dimensionless and scale-invariant. It is determined by the degree of spatial confinement of the field in the non-linear material. To an excellent approximation, it is independent of n_2 , the peak electric field amplitude, Q , and small deviations in ω . Let us denote by P_{IN}^S, P_{OUT}^S the steady-state values of P_{IN} and P_{OUT} respectively. Using a Lorentzian transmission spectrum in the linear case and perturbation theory for small $\delta n(\mathbf{r})$, we obtain:

$$\frac{P_{OUT}^S}{P_{IN}^S} = \frac{T_P}{1 + \left(P_{OUT}^S / P_0 - \delta \right)^2}, \quad (2)$$

where $\delta = (\omega_{RES} - \omega) / (\gamma_w + \gamma_r)$, $T_P = [\gamma_w^2 / (\gamma_w + \gamma_r)^2]$ is the peak transmission, and P_0 is a ‘‘characteristic power’’ of this cavity given by:

$$P_0 \equiv \frac{\sqrt{T_P}}{\kappa Q^2 (\omega_{RES} / c)^{d-1} n_2(\mathbf{r})_{MAX}}. \quad (3)$$

According to Eq.(2), P_0 sets the power scale for observing bistability in a cavity of interest.

To check our analytical theory, we obtain $\kappa = 0.020$ from a single non-linear computation; together with the knowledge of Q and ω_{RES} , we obtain $P_{OUT}^S(P_{IN}^S)$ for $\delta = 3.2$ which we plot, as a solid line in Fig. 3. We compare our analytical theory with numerical experiments in which we launch smoothly turned-on CW signals into the cavity. To observe the upper hysteresis branch we launch large-amplitude and wide-width gaussian pulses that decay into smaller steady state CW values. The small discrepancy between our analytical theory and the numerical experiments in Fig. 3 is mostly attributable to the fact that the linear-regime transmission curve is not a perfect Lorentzian; we operate fairly close to the edge of the axial band-gap, and the linear transmission shape looks more like a ‘‘tilted’’ Lorentzian.

While numerical simulations for larger Q s would be prohibitively long, our analytical model allows us to predict the behavior of a high- Q device. According to Eq. (3), the power requirements drop with $1/Q^2$. Q can be increased by adding more spheres to the ‘‘walls’’ of the cavity. For Q of 6000 (which is still compatible with 10Gbit/sec signals), the non-linear index changes are < 0.001 (which is still compatible with nearly instantaneous non-linear materials, and below the damage threshold for many materials, including many Chalcogenide glasses [14]). The power needed to observe bistability is 34mW (assuming $n_2 = 1.5 * 10^{-17} m^2/W$, a value typical for the Chalcogenide glasses [14,15] that we envision using), which is fairly close to the 5mW single-channel peak power levels used in telecommunications. The power can be

further decreased by reducing the modal volume and/or by using materials with larger Kerr coefficient.

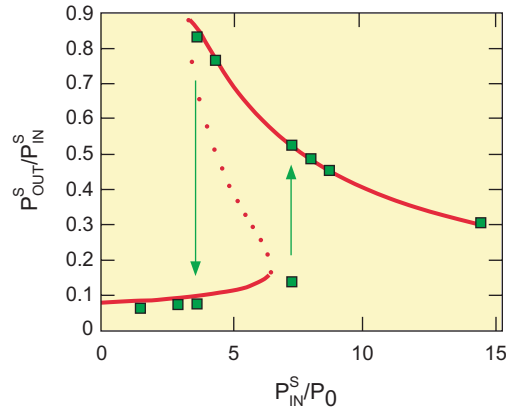


Fig. 3. Plot of the observed P_{OUT}^S vs. P_{IN}^S for the device from Fig. 1, when $\delta=3.2$. The squares are points obtained from numerical experiments. The line is the analytical prediction, which clearly matches the numerical experiments; the dotted part of the line is unstable and therefore physically unobservable.

There are two reasons why the required power is so small compared to other fiber systems that display optical bistability [16,17]. First, all the energy of the mode is concentrated in a very small modal volume; consequently, for the same amount of modal energy, the peak $\delta n(r)$ induced in the system is much larger than in other systems with much larger modal volumes [17]. This is manifested by the fact that the non-linear feedback parameter $\kappa=0.020$ is fairly large. (For comparison, if one had a system in which all the energy of the mode were contained uniformly inside a volume $(\lambda_0/2n_L)^3$, κ would be ≈ 0.15 .) Second, a large quality factor can be achieved at the same time as the large κ . Increasing Q while keeping other parameters fixed decreases the power requirements as $1/Q^2$ [18,19]. The first factor of Q appears because increasing Q for a fixed P_{IN} leads to a larger peak electric field inside the cavity, due to the longer energy accumulation. The second factor of Q comes from the fact that the resonance peak width is $\sim 1/Q$, thereby reducing the required frequency (index) shift by $1/Q$ as well.

In addition to inserting spheres into the core, there are many other possibilities for experimental implementation of the axial modulation. Conceptually, the fact that the guiding mechanism does not depend on the core and the fact that the core is initially hollow, provide for significantly more experimental flexibility in implementing a strong optical axial modulation than exists in conventional fibers. Other authors [20] demonstrated impressive manipulation of optical properties of holey fibers by inserting various kinds of materials into the holes, including producing periodic axial modulation of the core. Alternatively, one could perform photo-lithography on the inner surface of the core: a photoresist would be co-drawn as the inner-most layer of the cladding, laser beams shone from the side would implement cross-linking of the photo-resist, and then the hollow core would be used to transport all the acids and/or bases needed to etch a periodic structure onto the inner-most layer of the cladding.

Finally, for many applications, responses that more closely resemble step-functions than the one shown in Fig. 3 would be desired. In order to achieve this, one could use generalized Fabry-Perot filters which have flattened-top-Lorentzian linear transmission spectra.

3. Cutoff solitons in axially uniform photonic bandgap fibers

Gap solitons and optical switching [21-25] have been extensively studied in nonlinear dielectric structures with axial periodicity in their linear refractive properties. Corresponding experimental realizations include fiber Bragg gratings [26,27] and integrated multi-layer heterostructures [28]. Such systems exhibit spectral gaps of high reflectivity for wave-propagation along the axial direction. For intense light illumination at a frequency inside the gap they exhibit solitary wave solutions, called gap-solitons, and introduce a strong power-dependence to the transmissivity, in some cases resulting in to a bistable response. Such systems are very attractive for all-optical switching, logic-gate operation, memory etc.

Because of the necessity of an axial spectral gap for their existence, gap solitons have always been studied in axially periodic systems. In this section [29], we show that similar complex behavior is also possible in axially-uniform photonic bandgap (PBG) fibers [2,3,5,30]. We show that in the presence of an optical Kerr-type nonlinearity, axially-uniform PBG fibers exhibit gap-soliton-like generation and associated bistability. This nonlinear response is a direct consequence of the particular guided-mode dispersion relation, which involves a frequency cutoff at $k=0$: tuning the input frequency below the cutoff provides for an effective axial spectral-gap. This is particularly true, since there are minimal radiation losses (we operate far from the light line), resulting in a distributed feedback mechanism similar to a Bragg reflector. Also, stationary solutions with very low group velocities (even zero) come in naturally at $k=0$ [31]. We term these solitons “cutoff solitons” in order to distinguish them from all other gap solitons which have thus far only been described for axially *periodic* structures.

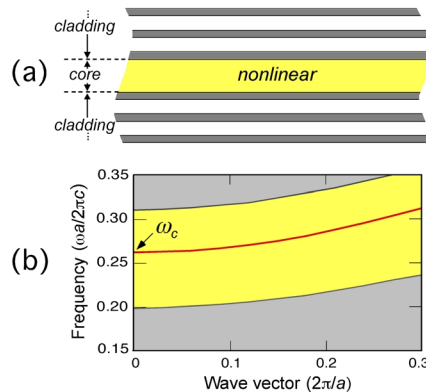


Fig. 4. (a) 2D simulation system: cladding consists of alternating dielectric layers of high-(2.8) and low-(1.5) index with thickness $0.3a$ and $0.7a$, where a is the period. The core diameter is $d=1.2a$ and index $n' = n_0 + n_2|E|^2$, where $n_0=1.6$. (b) Linear dispersion relations calculated by the FDTD method. The cutoff frequency is $\omega_c = 0.26215$. Gray areas represent cladding and radiation modes.

We study a 2D embodiment of PBG fibers, described in Fig. 4(a). This system captures the most essential features of the 3D fiber, including the guided-mode cutoff at $k=0$ and the absence of a complete spectral gap. In Fig. 4(b) we plot the guided mode dispersion relation in the linear (low-intensity) limit, as calculated by the finite-difference time-domain (FDTD) method. Any small change in linear refractive index will result in an almost constant frequency shift of the dispersion relations.

For input frequencies below the cutoff $\omega < \omega_c$ there are no available guided states in the core. Assume an input port consisting of a similar fiber with a higher-index core n' and cutoff frequency $\omega'_c < \omega_c$. Low-intensity incident guided waves with $\omega'_c < \omega < \omega_c$ will decay exponentially in the axial direction and result in a strong reflection. This is similar to waves

incident onto a Bragg reflector and is in contrast to *all* other axially uniform fibers. At high input power we observe a wide range of nonlinear phenomena, such as bistability and self-pulsing, similar to those found in nonlinear axially periodic gratings. We study these phenomena in the limit of small nonlinearities (which is the experimentally correct limit).

To explore these effects in detail, we perform time-domain simulations for the system shown in Fig. 4(a) using the FDTD method. Any choice of refractive indices and structural parameters for the linear input and output fibers suffices as long as $\omega'_c < \omega_c$. For example, enlarging the core area would have the desired effect. For simplicity we just use a higher-index core of $n'=1.9$. In Fig. 5 we plot the fiber's nonlinear response for two nonlinear-core lengths, $L=5a$ and $L=8a$. A CW excitation with $\omega'_c < \omega < \omega_c$ is the input for both cases. Fields and flux are monitored at the output while perfectly-matched-layer absorbing boundary conditions are used to simulate perfect absorption at the edges of the computational cell.

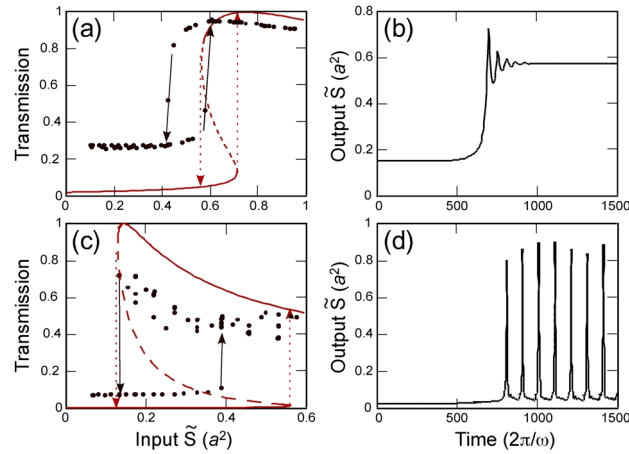


Fig. 5. (a) Transmission vs input flux \tilde{S} for the $L=5a$ system and $\alpha a/2\pi c=0.26$. The normalized flux \tilde{S} is defined as $\tilde{S} = n_0 \cdot n_2 \cdot S$, where S is the electromagnetic flux through the fiber's cross section. Both 2D FDTD (dots) and 1D model (red line) results are shown. The unstable solutions (physically unobservable) of the 1D model are represented by the dashed line. (b) Output flux during switch-up (path marked by the up-pointing arrow) for the $L=5a$ system. (c) and (d) Same as (a) and (b), but for the $L=8a$ system.

We obtain two types of response: i) CW: observed in the smaller $L=5a$ system, involving bistable switching between a CW low- and a CW high-transmission state (Figs. 5a and 5b). ii) Pulsating: observed in the larger $L=8a$ system, involving bistable switching between a stable low- and a pulsating high-transmission state (Figs. 5c and 5d). Such dual response is well known in grating nonlinear systems. The steady state is the result of the excitation of a stationary gap-soliton-like object in the structure. In Fig. 6(b) we plot the field intensity profile along the nonlinear core for the resonant transmission point. While a similar output response could also be obtained in a simple nonlinear slab [32], there are very important differences. In a nonlinear slab, low-intensity propagation is allowed, nonlinear feedback occurs entirely at the boundaries, and bistability results from an intensity-dependent frequency-shift of the resonant transmission condition. In our case low-intensity propagation is prohibited (as shown in Fig. 6(b)), and thus nonlinear feedback is axially distributed throughout the nonlinear fiber. This is achieved because we operate below cutoff while having minimal coupling to radiation modes (possible at $k=0$), and thus is equivalent to operating in a gap. Bistability results from gap-soliton-like excitations, which share very similar physics with gap

solitons in nonlinear Bragg gratings. Since they appear in an axially uniform system, however, we term them “cutoff solitons” in order to distinguish them.

The transition from a steady solution to a pulsating one is related to the cutoff soliton becoming non-stationary [25]. The excited cutoff soliton then propagates along the core resulting in an output that consists of a periodic series of pulses. This alternative (convective) method of energy transfer, nevertheless, also results in high transmission. Our axially-uniform nonlinear system, thus, overall responds similarly to a nonlinear Bragg grating.

The key feature common between our system and a Bragg grating is the cutoff, or gap, of the dispersion relations, found only at $k=0$ in our case. We create a 1D model where the dispersion relations are fit to quadratic forms that include the nonlinear shift $\delta\omega$:

$$\omega(|E|^2, k) = \omega_c + \alpha \cdot k^2 + \delta\omega(|E|^2), \quad \omega'(k) = \omega'_c + \alpha' \cdot k^2 \quad (4)$$

for the nonlinear and linear core regions respectively. We write the field in the nonlinear core as the product of a normalized transverse distribution $F(x, y)$ and a slowly-varying amplitude

$A(z, t)$, $E(r, t) = \frac{1}{2} \{F(x, y)[A(z, t)e^{ik_0 z}]e^{-i\omega_0 t} + c.c.\}$, where z is the axial direction. From first order perturbation theory in small nonlinearities, we find (similar to Eq. (1)) [33]:

$$\delta\omega(z) = -\frac{\omega_0 \int n_2(x, y)n_0(x, y)(|F \cdot F|^2 + 2|F|^4) dx dy}{4 \int n_0(x, y)^2 |F|^2 dx dy} |A(z)|^2 \equiv -\gamma |A(z)|^2, \quad (5)$$

where the integral is performed over the total cross-sectional area. Eq. (5) is the general 3D expression. The nonlinear coefficient γ is calculated using the FDTD method as $\gamma \equiv 0.02 \cdot n_0 \cdot n_2|_{\max}$ at $\omega_0 = \omega_c$. It is a weakly increasing function of frequency, but for simplicity we assume it constant. Other parameters used are $\omega_c = 0.26215(2\pi c/a)$ [$\omega'_c = 0.244(2\pi c/a)$] and $\alpha = 0.564(ac/2\pi)$ [$\alpha' = 0.463(ac/2\pi)$].

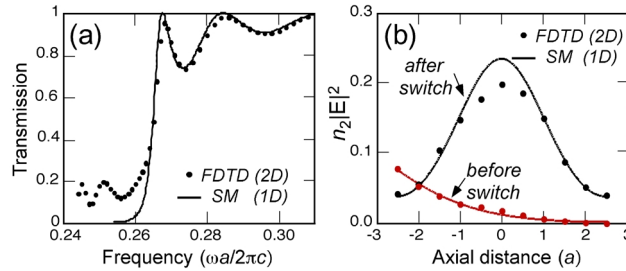


Fig. 6. (a) Linear transmission coefficient vs frequency for the $L=5a$ system. (b) Normalized intensity (or local index change $\delta n = n_2 |E|^2$) along the nonlinear core for the $L=5a$ system.

We first calculate the predicted frequency dependence of the *linear* transmission coefficient for the $L=5a$ system. This is plotted in Fig. 6(a) along with the full-2D FDTD data. Excellent agreement is found above cutoff. Note that the 1D model does show structure below cutoff, because it ignores the small coupling with the cladding modes (gray areas in Fig. 4(b)). This coupling could be further suppressed by reducing the index contrast between the different segments.

In Figs. 5(a) and 5(c) we plot the high intensity predictions of the 1D model along with the full-2D nonlinear FDTD data. Considering the simplicity of the 1D model, the general agreement is surprisingly good. The differences in switching intensities can be attributed to neglecting the frequency dependence of γ ; neglecting second order corrections in γ ; and to nonzero contributions from cladding modes. In Fig. 6(b) we plot the intensity along the nonlinear core for the $L=5a$ system at two different points: at the peak of the upper transmission branch where a cutoff soliton has been excited, and at the lower branch where the

wave decays exponentially; the 1D model captures all the essential features of the 2D system's nonlinear response.

We next derive an analytic expression for the slowly varying amplitude A . In frequency domain, the equation for $\tilde{A}(z, \omega - \omega_c)$ is $\partial^2 \tilde{A} / \partial z^2 + k^2 \tilde{A} = 0$, where we expand around the cutoff frequency ω_c , and k contains the nonlinear index change (first order terms vanish at cutoff). Using the dispersion relations of Eq. (1), $k^2 = (\omega - \omega_c - \delta\omega) / \alpha$, and transforming back into the time domain we arrive at the nonlinear Schrödinger equation¹⁴ (NLSE):

$$\frac{\partial A}{\partial t} - i\alpha \frac{\partial^2 A}{\partial z^2} - i\gamma |A|^2 A = 0. \quad (6)$$

This is the same equation as the one derived for 1D nonlinear periodic systems [23] (with α the curvature of the band edge). The main similarity between the two systems is the form of the dispersion relations, and the existence of a gap. The latter is the marked difference between cutoff solitons and usual nonlinear fiber solitons, along with that cutoff solitons can have *any* arbitrary group velocity, even zero. Any nonlinear system with similar dispersion relations is thus well described by Eq. (6). Such systems include metallic waveguides, multilayer stacks, PBG fibers, and photonic crystal linear-defect waveguides.

To summarize, we presented an axially uniform nonlinear system that exhibits gap-soliton-like formation and associated switching. The most important quality of this system is the special nature of the dispersion relations of the guided modes, involving a frequency cutoff at zero wavevector. In practical experimental setups these solitons will physically behave, in the vast majority of cases, the same as gap solitons. We term these solitons "cutoff solitons" to distinguish them from the usual gap solitons appearing in axially periodic systems. The ability to obtain gap-soliton-like formation without imposing axial periodicity leads to new design and fabrication opportunities for eventual experimental realization of all-optical devices.

4. Conclusion

As demonstrated, non-linear photonic bandgap in-fiber devices can be used to explore some very interesting parameter regimes of operation that were inaccessible before. In particular, ultra-fast optical bistability is possible in such devices, even at very small power levels, and very small device-sizes. Moreover, photonic bandgap fibers also enable (for the first time) observation of gap-like solitons in axially uniform structures.

Acknowledgments

Help is gratefully acknowledged from S. Jacobs, T. Engeness, O. Weisberg, M. Skorobogatiy, and E. Ippen. We also thank B. J. Eggleton and J. E. Sipe for suggesting the name "cutoff solitons" and S. Trillo, F. Kaertner, and Y. S. Kivshar for useful discussions and physical insight. This research was supported in part by, the U.S. Army through the Institute for Soldier Nanotechnologies, under Contract DAAD-19-02-D0002 with the U.S. Army Research Office, and the Materials Research Science and Engineering Center program of the NSF under Grant No. DMR-9400334. This material is based upon work supported by the NSF under Grant No. 0123460.